

# Numerical investigation of the transmission route of infectious particles produced by human

Wonseok Oh <sup>a</sup>, Ryoza Ooka <sup>b</sup>, Hideki Kikumoto <sup>c</sup>, Sihwan Lee <sup>d</sup>

<sup>a</sup> Institute of Industrial Science, The University of Tokyo, Tokyo, Japan, oh-ws@iis.u-tokyo.ac.jp

<sup>b</sup> Institute of Industrial Science, The University of Tokyo, Tokyo, Japan, ooka@iis.u-tokyo.ac.jp

<sup>c</sup> Institute of Industrial Science, The University of Tokyo, Tokyo, Japan, kkmt@iis.u-tokyo.ac.jp

<sup>d</sup> Department of Architecture, Shinshu University, Japan, shany@shinshu-u.ac.jp

**Abstract.** This study aims to investigate the major factors to influence the respiratory transmission occurred by infectious particles from a human in an indoor environment. Identifying the critical factors of respiratory transmission is important for taking a countermeasure to control its spread. However, it is difficult to track large numbers of infectious particles generated by a human and floating in a room by the experimental method. Therefore, the transient jet airflow by human cough was numerically reproduced, and the trajectories of particles were investigated using the Lagrangian method. In the numerical analysis, two persons sitting and facing each other in a small office room were considered assuming that one person produced infectious particles by cough, and another was exposed to the infection. The trajectory of the dispersed infectious particles was calculated to confirm the proportion of particles that were directly inhaled by a person, attached to the human body surface, adhered to the floor, removed by ventilation, and suspended in the air. Also, the size of particles (1, 5, 10, 20, 40, and 80  $\mu\text{m}$ ) produced by the infector, the ventilation rate ( $6 \text{ m}^3 \text{ h}^{-1}\text{-person}^{-1}$ , equivalent to air changes per hour is  $0.5 \text{ h}^{-1}$ ), and the distance between individuals (0.9 m (3 ft) and 1.8 m (6 ft)) were investigated as an influential major factor to affect the spread of transmission. As a result, it was confirmed that the effects of gravity and inertia increased with larger particles, resulting in a greater rate of adhered particles to the floor. On the other hand, when the size of particles was smaller, they were able to be removed more effectively by increasing the ventilation rate. Further, when the individuals were spaced 1.8 m apart, particles larger than 20  $\mu\text{m}$  had no significant effect on droplet transmission. However, the smaller particles less than 10  $\mu\text{m}$  were highly likely to be inhaled directly and cause droplet transmission. Therefore, for smaller particles less than 10  $\mu\text{m}$ , practical measures to avoid infections such as social distancing is necessary.

**Keywords.** droplet dispersion, Lagrangian method, coughing, breathing, particle fate

**DOI:** <https://doi.org/10.34641/clima.2022.411>

## 1. Introduction

Our lives are severely affected by the risk of infection during the coronavirus disease 2019 (COVID-19) pandemic, which is caused by the SARS-CoV-2 virus. Infectious respiratory diseases have severe negative effects on public health, society, and the economy. Various types of respiratory viruses are known, such as the measles virus, influenza A virus, respiratory syncytial virus, rhinoviruses, coronaviruses, and adenoviruses. Respiratory diseases can be spread via naturally produced droplets and droplet nuclei from an infected person by breathing, speaking, coughing, and sneezing. The droplets consist of 98.2%  $\text{H}_2\text{O}$  and 1.8% nuclei (mass ratio) [1], and small droplets evaporate

quickly and become droplet nuclei. Respiratory viruses can be spread via three transmission routes: contact (direct or indirect), droplet, and airborne transmission [2,3]. Washing hands and wearing masks are effective ways to prevent contact and droplet transmission [4,5]. However, it is known that droplet nuclei smaller than 5  $\mu\text{m}$  may remain in the air for a long time, causing airborne infection [2]. Samples of SARS-CoV-2 RNA have recently been detected in the air and on the surfaces in COVID-19 wards [6,7]. However, although direct evidence of an infectious infection is difficult to obtain, Yu et al. presented reasonable evidence of aerosol infection by showing the predictability of viral infections through analyses of airflow and contaminant dispersion using computational fluid dynamics (CFD)

[8]. Zhu and Kato examined the diffusion characteristics of droplets of various sizes using CFD [9]. Droplets with a diameter of less than or equal to 30  $\mu\text{m}$  ( $d_p \leq 30 \mu\text{m}$ ) were affected very little by inertia and gravity and tended to diffuse randomly into the room. Wan et al. experimentally investigated the importance of mechanical ventilation in reducing respiratory infection risk in a hospital ward [10].

The characteristics of airflow, droplets, and droplet nuclei can be used to understand and predict the spread of infection. Gupta and colleagues measured subjects' airflow characteristics during breathing and talking [11] and proposed flow rate model coughing [12]. Several researchers tried to measure the maximum air velocity and direction produced by coughing using the particle image velocimetry (PIV) technique [13,14]. Recently, an attempt has been made to analyze the distribution of airflow caused by coughing [15]. The flow rate variations during coughing and breathing could be represented as a combination of gamma probability distributions and sine waves, respectively. Xie et al. inferred the size distribution of droplets produced by coughing and talking using an experimental method [16]. Additionally, the particle size distributions of subjects were confirmed by Chao et al. for coughing and speaking [13] and by Johnson et al. for breathing [17]. Nishimura et al. employed PIV to visualize the movement of particles released by coughing and sneezing and measured the dynamics of droplets and droplet nuclei [18].

Using a simple physical model, Xie et al. estimated how far droplets produced by various respiratory activities can travel [19]. The maximum distances were 6, 2, and 1 m for sneezing, coughing, and breathing, respectively. The maximum distance traveled by droplets can be used as a reference index for social distancing, which can be used to avoid the spread of infection. Liu et al. developed a theoretical model that can be used to estimate the size and dispersion of droplets and droplet nuclei considering evaporation [20]. The droplets became droplet nuclei with 32% of their initial size by evaporation.

CFD analysis is most commonly used to understand the dispersion of droplets and droplet nuclei. The dispersion of cough droplets and droplet nuclei considering evaporation was investigated and validated by CFD analysis using the Eulerian-Lagrangian method [21,22]. Yang et al. investigated the dispersion of droplets in a crowded bus to understand the ventilation effectiveness and effects of environmental factors [23]. Zhang and Li investigated the dispersion of droplets from a coughing person in a rail cabin. They found that increasing the air changes per hour (ACH) was not the best way to reduce the risk of airborne infection [24]. Higher-velocity air movement delivers droplets and droplet nuclei more rapidly and diffuses them more widely, exposing more people to

the risk of infection.

The most important factor for preventing airborne infection in an indoor environment is maintaining a high ventilation rate to quickly remove potentially infectious particles. Mui et al. investigated the dispersion and diffusion of droplet nuclei 0.1 and 10  $\mu\text{m}$  in size in an indoor environment under displacement ventilation and mixing ventilation conditions [25]. They used a drift flux model to calculate the distribution of the droplet nuclei concentration in the room and estimate the infection risk. Zhao and Wu evaluated the deposition of particles on indoor surfaces experimentally and verified the results by comparison with numerical analysis [26]. In addition, various ventilation systems were reviewed using numerical analyses to investigate airborne infection [27,28]. However, most studies utilized the drift flux model to confirm the distribution of droplets and droplet nuclei. Therefore, it is necessary to track the route of infectious particles and confirm the fate of the particles for identifying the key factors of the infection route and taking a countermeasure against infectious diseases in an indoor environment.

## 2. Methodology

### 2.1 Eulerian model

The three-dimensional transient Reynolds-averaged Navier-Stokes equations for the conservation of mass, momentum, and energy of a continuous fluid inside a room were solved using the realizable  $k-\epsilon$  model as summarized in **Tab. 1** [29].

A second-order upwind scheme was used as the convection term in the discretization scheme. The pressure-velocity coupling for the continuous fluid was solved using the SIMPLE algorithm [30]. The realizable  $k-\epsilon$  model has been used and validated in many previous studies to investigate particle dispersion and shown to agree well with experimental results [31-34].

**Tab. 1** - Numerical methods used for simulation.

Commercial code	STAR-CCM+ ver. 14.06
Turbulence model	Realizable $k-\epsilon$ model
Convection	Second-order upwind scheme
Solver	SIMPLE algorithm
Buoyancy	Boussinesq approximation
Particles	Lagrangian model
Mesh	Polyhedral with prism layer mesh (approx. 1,100,000 cells)
Time	Implicit unsteady state ( $dt = 0.05 \text{ s}$ )

## 2.2 Lagrangian model for particles (droplet and droplet nuclei)

The dispersion of particles in the continuous fluid was calculated using the Lagrangian model. The conservation of the linear momentum of the particle is balanced by the surface and body forces. This study considered the drag ( $\vec{F}_D$ ), pressure ( $\vec{F}_P$ ), and gravitational forces ( $\vec{F}_G$ ) as expressed in Equations (1)–(4).

$$m_p \frac{d\vec{u}_p}{dt} = \vec{F}_D + \vec{F}_P + \vec{F}_G \quad (1)$$

$$\vec{F}_D = \frac{1}{2} \frac{C_D}{C_C} \rho_f A_p |\vec{u}_f - \vec{u}_p| (\vec{u}_f - \vec{u}_p) \quad (2)$$

$$\vec{F}_P = -V_p \nabla P \quad (3)$$

$$\vec{F}_G = V_p (\rho_p - \rho_f) \vec{g} \quad (4)$$

Here,  $m_p$  is the particle mass;  $\vec{u}_f$  and  $\vec{u}_p$  are the continuous velocity vectors of the fluid and particle, respectively, and  $\rho_f$  and  $\rho_p$  are the density of the continuous fluid and particle, respectively.  $A_p$  is the projected area, and  $V_p$  is the volume of the particle.  $\nabla P$  is the gradient of the static pressure in the continuous fluid, and  $\vec{g}$  is the gravitational acceleration vector.

The Schiller–Naumann correlation [35] was used to calculate the drag coefficient of the particle ( $C_D$ ) in Equation (5).  $C_D$  depends on the Reynolds number of the particle ( $Re_p$ ) in Equation (6). The Cunningham slip correction factor ( $C_C$ ) for droplets in small size was defined in Equation (7). The Cunningham effect occurs on particles smaller than 10  $\mu\text{m}$ .

$$C_D = \begin{cases} \frac{24}{Re_p} (1 + 0.15 Re_p^{0.687}), & Re_p \leq 10^3 \\ 0.44, & Re_p > 10^3 \end{cases} \quad (5)$$

$$Re_p = \frac{\rho_f d_p |\vec{u}_f - \vec{u}_p|}{\mu_f} \quad (6)$$

$$C_C = 1 + \frac{2\lambda}{d_p} \left( 1.257 + 0.4 \exp\left(-\frac{1.1 d_p}{2\lambda}\right) \right) \quad (7)$$

Where  $d_p$  is the particle diameter, and  $\mu_f$  is the dynamic viscosity of the continuous fluid.  $\lambda$  is the mean free path of the air molecular (i.e.  $\lambda = 0.0673 \mu\text{m}$  at 23 °C and 1 atm air [36]).

In the simulation, the turbulent dispersion of particles was considered because turbulent motion significantly affects the particles with small sizes. The stochastic model similar to the random walk model was used [37]. The velocity of the continuous fluid ( $\vec{u}_f$ ) was calculated by adding the fluctuating velocity component ( $\vec{u}'_f$ ) to the local Reynolds-averaged velocity of the continuous fluid ( $\vec{u}_f$ ), as shown in Equation (8). The fluctuating velocity component was randomly sampled by the Gaussian

probability density function ( $p$ ) with the standard deviation ( $\sigma = \sqrt{2k/3}$ ) and zero mean in Equation (9) [9]. Here,  $k$  is the turbulent kinetic energy.

$$\vec{u}_f = \vec{u}_f + \vec{u}'_f \quad (8)$$

$$p(\vec{u}'_f) = \frac{1}{\sqrt{2\pi}\sigma^2} \exp\left(-\frac{\vec{u}'_f{}^2}{2\sigma^2}\right) \quad (9)$$

## 2.3 Case study description

Indoor space of the typical small office with a size of 3.6 × 2.7 × 2.5 m<sup>3</sup> (width × length × height) was considered for the simulation. Mechanical ventilation by the displacement ventilation system was investigated as illustrated in Fig. 1. The ventilation rate was set as 6 m<sup>3</sup> h<sup>-1</sup>·person<sup>-1</sup>, and two occupants were considered (equivalent ACH is 0.5 h<sup>-1</sup>). One was assumed as an infected person and the other was set as a susceptible person. Two thermal manikins in a seated position with a height of 1.21 m were placed in the center of the room. The furniture was not considered because its various types and locations can interfere an indoor airflow and may have a significant effect on the results [38]. The present study analyzed the independent influence of the infectious particles generated from the person.

Further, different cases of social distancing were investigated as an influential major factor to affect the spread of the transmission by setting the several distances between individuals (Case A: 0.9 m (3 ft) and Case B: 1.8 m (6 ft)). The distances between individuals were modeled by measuring nose-to-nose distance.

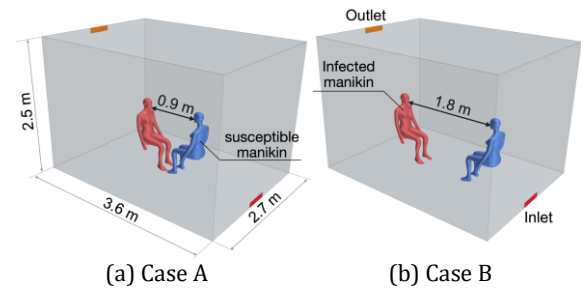


**Fig. 1** - Different cases of social distancing in a typical small office.

The detailed boundary conditions for the calculation can be found in Tab. 2. A boundary condition of velocity inlet was applied for the inlet of the room. Supplying air temperature was set at 18 °C. The opening of the inlet and outlet were assumed to have the same size of 0.45 × 0.1 m<sup>2</sup>. The outlet was a pressure outlet with zero static pressure. The constant temperature of 24 °C was set to all indoor walls. The boundary condition of the infected and susceptible manikins was set as a constant heat flux of 23 W/m<sup>2</sup>.

For coughing and breathing behaviors, boundary condition at the mouth opening was set as velocity inlet, and a time-series velocity profile for each behavior was applied. The temperature of the airflow due to exhalation was set at 34 °C, and a turbulence intensity was set at 10% [39]. Validation calculations were conducted to determine a statistically appropriate number of particles, and for this simulation, 5,000 particles were chosen for each size.

**Tab. 2** – Boundary conditions.

Inlet opening	velocity inlet: according to 1.0 ACH temperature: 18 °C turbulence intensity: 5% turbulence length scale: 7% of hydraulic diameter $d_h$ size: $0.45 \times 0.1 \text{ m}^2$
Outlet opening	pressure outlet: static pressure = 0 size: $0.45 \times 0.1 \text{ m}^2$
Wall	Dirichlet condition, $T_w = 24 \text{ °C}$ two-way all- $y^+$ wall treatment no-slip boundary condition
Surface of infected / susceptible manikin	Neumann condition, $q_s = 23 \text{ W/m}^2$ two-way all- $y^+$ wall treatment no-slip boundary condition
Mouth opening of infected / susceptible manikin	velocity inlet <ul style="list-style-type: none"> <li>• infected manikin: cough airflow at first time and follow the breath cycle (equation (10))</li> <li>• susceptible manikin: follow the breath cycle (equation (10))</li> </ul> temperature: 34 °C turbulence intensity: 10% turbulence length scale: 7% of $d_h$
Particles	$d_p$ : 1, 5, 10, 20, 40, and 80 $\mu\text{m}$ 5,000 particles for each size

## 2.4 Boundary conditions for particles

The deposition on the surface is a major removal mechanism of particles, and thus, stick condition on the floor, and the surface of infected and susceptible manikins was considered [40]. The ceiling and vertical walls were set as a rebound condition. An escape condition was applied to the outlet opening and mouth openings of infected and susceptible manikins, and the fate of particles was tracked.

## 2.5 Cough model for infected manikin

The direction of the cough airflow was set to 27.5 °

downward as shown in **Fig. 2**, and the time-series velocity profile obtained from the experiment [41] was adopted as the boundary condition in the mouth of the infected manikin (**Fig. 2(b)**).

Water droplets quickly equilibrate with the surrounding environment and its evaporation process is very rapid. The equilibrium size of the droplet is reduced to about half its initial expiratory size [42]. In this study, the size of the droplet in the equilibrium state, not the initial size of the droplet, was considered to reduce the computational load in the calculation, and the evaporation process was not conducted.

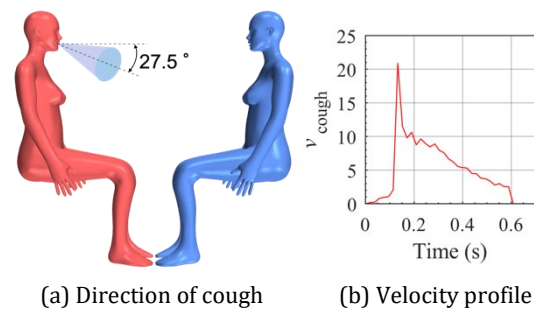


**Fig. 2** – Cough model for infected manikin.

## 2.6 Breath model for infected and susceptible manikin

In the breath model, the airflow rate of inhalation and exhalation was assumed to be a sine wave. Tidal breath flow rate (inhalation or exhalation) and its frequency were assumed as 1 L and 3 s, respectively, as described in Equation (10). The mouth opening area of 123 mm<sup>2</sup> was considered, and the infected manikin started coughing at the beginning of the simulation calculation and the coughing was last for 0.6 s. Further, during the simulation, the breath model was started after the cough model was completed.

$$V_{\text{breath}}(t) = \frac{\pi}{6} \sin\left(\frac{\pi}{3}t\right), [\text{L/s}] \quad (10)$$

## 2.7 Validation of proper number of particles

It is necessary to set a proper number of particles for statistical analysis for the Lagrangian simulation. The motion of the particle is greatly affected by turbulence as the particle size is smaller. Therefore, the appropriate number of particles was investigated firstly with the particle size of 1  $\mu\text{m}$ , and the same number of particles was applied to all particles. Various numbers of particles of 1,000, 5,000, 10,000, and 20,000 were considered, and the ratio of the time series particle fates to the initial number of particles was confirmed. There were no significant differences in more than 5,000 particles, and thus, 5,000 particles were investigated in this study.

### 3. Results and Discussion

#### 3.1 Indoor Airflow distribution

Fig. 3 displays the results of indoor airflow distributions during the coughing and breathing stage. The rising airflows due to the heat of the human body were formed adjacent to both manikins. The velocity of cough airflow showed over 10 m/s at 0.2 s. Also, the formed exhaled airflow by breathing can be confirmed at 2.0 s after the infected manikin finished the coughing behavior. The respiratory airflow of susceptible manikin was directed forward, but the expiratory airflow was warmer than the ambient air temperature and raised due to the buoyancy effect.

In Case A (social distancing with 0.9 m), the airflow by coughing tended to reach the susceptible manikin. However, when the social distancing was doubled in Case B (1.8 m), it was difficult to reach the airflow to the opponent.

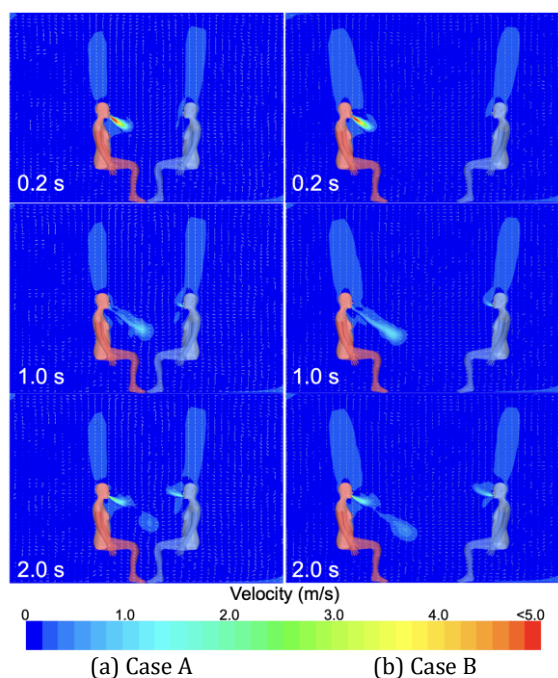


Fig. 3 - Indoor airflow distribution with cough and breath model.

#### 3.2 Particle dispersion in the room

Fig. 4 shows the results of particle dispersion generated by coughing behavior over time. In Case A (social distancing with 0.9 m), the released particles reached the opponent's body around 5 seconds after coughing. However, when the social distancing was doubled to 1.8 m in Case B, particles did not reach the opponent. Also, it was found that particles with large sizes such as 80  $\mu\text{m}$  headed to the bottom relatively quickly. On the other hand, particles of small size such as 1.0  $\mu\text{m}$  descended more slowly and tended to rise along the thermal plume of the body.

The upward airflow by the human body was greater in Case A where two occupants were set closer to each other than Case B, showing a tendency that particles smaller than 40  $\mu\text{m}$  were more easily to rise to the ceiling and diffuse into the room.

During the simulation from 100 seconds to 300 seconds, particles of 20  $\mu\text{m}$  or less suspended in the air were gradually removed by deposition on the floor, exhaust by ventilation, adhesion to the human body surface, and intake by respiration.

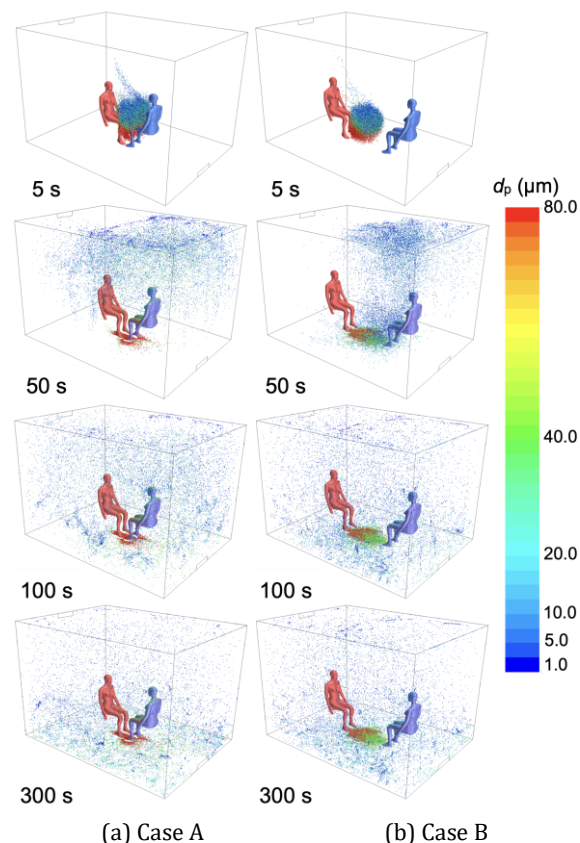


Fig. 4 - Results of particle dispersion in each case of social distancing in a typical small office.

#### 3.3 Calculated particle fates

Tab. 3 shows the fates of infectious particles generated by coughing after 300 seconds of the simulation according to the particle sizes and distances between individuals. To understand the characteristics of the movement path by the particle sizes, the ratio for each particle size was analyzed.

The smaller size of particles tended to float and be suspended in the room regardless of the distance between individuals. The larger size of particles showed to easily deposit on the surface of the floor ( $F$ ) or susceptible body ( $S_{sk}$ ).

In case of a short social distancing (0.9 m in Case A) between two persons, 45.5% of the 40  $\mu\text{m}$  size of the particles and 38.1% of the 80  $\mu\text{m}$  size of the particles generated from the infected person were

deposited on the susceptible manikin ( $S_{sk}$ ) and 39.8% on the floor ( $F$ ). However, when the distance between individuals became doubled, only 4.8% of the 40  $\mu\text{m}$  size of particles were attached to the surface of the susceptible manikin ( $S_{sk}$ ), the 80  $\mu\text{m}$  size of the particles could not reach the surface of the susceptible manikin ( $S_{sk}$ ), and most of the particles (94.4–97.7%) were removed by deposition to the floor ( $F$ ).

The droplet transmission and airborne transmission by ingestion of infectious particles ( $S_m$ ) could occur when the particle size was less 40  $\mu\text{m}$ , however, the probability of transmissions was not significantly influenced by the distance between individuals and size of particles. However, as the distance between individuals increases, range of particle sizes, which can cause the droplet and airborne transmissions, could be reduced.

In general, infectious particles can be removed by the exhaust by ventilation and deposition on the floor. However, regular sterilization should be carried out to prevent a contact transmission possibly occurring by the deposited infectious particles. Also, particles smaller than 20  $\mu\text{m}$  tend to be suspended in the air for a long time, hence, they should be rapidly removed by increasing the ventilation rate and the utilization of the air purifier to lower the risk of airborne transmission.

**Tab. 3** - Particle fates released from infected manikin for 300 s.

Distance (m)	$d_p$ ( $\mu\text{m}$ )	$I_{sk}$ (%)	$I_m$ (%)	$S_{sk}$ (%)	$S_m$ (%)	$E$ (%)	$F$ (%)	$A$ (%)
0.9	1	1.9	0.1	9.2	0.5	1.0	7.9	79.4
	5	1.5	0.1	9.3	0.8	0.8	17.5	70.0
	10	0.8	0.2	9.6	0.9	1.0	37.5	50.0
	20	1.1	0.2	14.0	0.7	0.5	66.5	17.1
	40	5.5	0.5	45.5	0.7	-	46.8	1.0
	80	21.9	0.1	38.1	-	-	39.8	0.1
1.8	1	2.1	0.2	6.2	0.7	2.2	4.3	84.3
	5	1.7	0.1	6.6	1.0	2.8	10.6	77.2
	10	1.2	0.1	7.6	0.8	1.7	28.7	59.9
	20	0.7	0.1	13.3	0.9	0.5	67.7	16.8
	40	0.8	-	4.8	-	-	94.4	-
	80	2.2	0.1	-	-	-	97.7	-

Note:  $d_p$  is the diameter of the particle, and  $I$  and  $S$  represent the infected and susceptible manikins. Subscripts of sk and m indicate the particles attached to the surface of the manikins and the particles inhaled by respiration, respectively.  $E$ ,  $F$ , and  $A$  represent discharged particles by outlet opening by ventilation, deposited particles on the floor, and suspended particles in the air, respectively.

## 4. Conclusion

This study investigated the probability of exposure to the respiratory infection of a susceptible person by tracking the spread of infectious particles caused

by the coughing of an infected person in a ventilated indoor office. As a result, it was found that the arrival of infectious particles can be significantly prevented when the distance between the individuals is maintained from 0.9 m to 1.8 m. Also, the small size of infectious particles capable of causing airborne transmissions was independent of the distance between individuals. Therefore, further studies are necessary to explore the countermeasures against airborne transmissions by appropriately increasing the ventilation rate and the utilization of air purifiers.

## 5. Acknowledgement

This work was supported by the Japan Society for the Promotion of Science (JSPS) KAKENHI Grant Number 21K18763.

## 6. References

- [1] M. Nicas, W.W. Nazaroff, A. Hubbard, Toward understanding the risk of secondary airborne infection: Emission of respirable pathogens, *J. Occup. Environ. Hyg.* 2 (2005) 143–154.
- [2] J.S. Kutter, M.I. Spronken, P.L. Fraaij, R.A. Fouchier, S. Herfst, Transmission routes of respiratory viruses among humans, *Curr. Opin. Virol.* 28 (2018) 142–151.
- [3] Y. Bu, R. Ooka, H. Kikumoto, W. Oh, Recent research on expiratory particles in respiratory viral infection and control strategies: A review, *Sustain. Cities Soc.* (2021) 103106.
- [4] P. Anfinrud, V. Stadnytskyi, C.E. Bax, A. Bax, Visualizing Speech-Generated Oral Fluid Droplets with Laser Light Scattering, *N. Engl. J. Med.* 382 (2020) 2061–2063.
- [5] K.F. Ho, L.Y. Lin, S.P. Weng, K.J. Chuang, Medical mask versus cotton mask for preventing respiratory droplet transmission in micro environments, *Sci. Total Environ.* 735 (2020) 139510.
- [6] K. Razzini, M. Castrica, L. Menchetti, L. Maggi, L. Negroni, N. V. Orfeo, A. Pizzoccheri, M. Stocco, S. Muttini, C.M. Balzaretto, SARS-CoV-2 RNA detection in the air and on surfaces in the COVID-19 ward of a hospital in Milan, Italy, *Sci. Total Environ.* 742 (2020) 140540.
- [7] A. Kenarkoohi, Z. Noorimotlagh, S. Falahi, A. Amarloei, S.A. Mirzaee, I. Pakzad, E. Bastani, Hospital indoor air quality monitoring for the detection of SARS-CoV-2 (COVID-19) virus, *Sci. Total Environ.* 748 (2020) 141324.
- [8] I.T.S. Yu, Y. Li, T.W. Wong, W. Tam, A.T. Chan, J.H.W. Lee, D.Y.C. Leung, T. Ho, Evidence of airborne transmission of the severe acute

- 
- respiratory syndrome virus, *N. Engl. J. Med.* 350 (2004) 1731–1739.
- [9] S. Zhu, S. Kato, J.H. Yang, Study on transport characteristics of saliva droplets produced by coughing in a calm indoor environment, *Build. Environ.* 41 (2006) 1691–1702.
- [10] M.P. Wan, C.Y.H. Chao, Y.D. Ng, G.N. Sze To, W.C. Yu, Dispersion of expiratory droplets in a general hospital ward with ceiling mixing type mechanical ventilation system, *Aerosol Sci. Technol.* 41 (2007) 244–258.
- [11] J.K. Gupta, C.H. Lin, Q. Chen, Flow dynamics and characterization of a cough, *Indoor Air.* 19 (2009) 517–525.
- [12] J.K. Gupta, C.H. Lin, Q. Chen, Characterizing exhaled airflow from breathing and talking, *Indoor Air.* 20 (2010) 31–39.
- [13] C.Y.H. Chao, M.P. Wan, L. Morawska, G.R. Johnson, Z.D. Ristovski, M. Hargreaves, K. Mengersen, S. Corbett, Y. Li, X. Xie, D. Katoshevski, Characterization of expiration air jets and droplet size distributions immediately at the mouth opening, *J. Aerosol Sci.* 40 (2009) 122–133.
- [14] S.-B. Kwon, J. Park, J. Jang, Y. Cho, D.-S. Park, C. Kim, G.-N. Bae, A. Jang, Study on the initial velocity distribution of exhaled air from coughing and speaking, *Chemosphere.* 87 (2012) 1260–1264.
- [15] M. Han, R. Ooka, H. Kikumoto, W. Oh, Y. Bu, S. Hu, Measurements of exhaled airflow velocity through human coughs using particle image velocimetry, *Build. Environ.* 202 (2021) 108020.
- [16] X. Xie, Y. Li, H. Sun, L. Liu, Exhaled droplets due to talking and coughing, *J. R. Soc. Interface.* 6 (2009).
- [17] G.R. Johnson, L. Morawska, Z.D. Ristovski, M. Hargreaves, K. Mengersen, C.Y.H. Chao, M.P. Wan, Y. Li, X. Xie, D. Katoshevski, S. Corbett, Modality of human expired aerosol size distributions, *J. Aerosol Sci.* 42 (2011) 839–851.
- [18] H. Nishimura, S. Sakata, A. Kaga, A new methodology for studying dynamics of aerosol particles in sneeze and cough using a digital high-vision, high-speed video system and vector analyses, *PLoS One.* 8 (2013).
- [19] X. Xie, Y. Li, A.T.Y. Chwang, P.L. Ho, W.H. Seto, How far droplets can move in indoor environments – revisiting the Wells evaporation–falling curve, *Indoor Air.* 17 (2007) 211–225.
- [20] L. Liu, J. Wei, Y. Li, A. Ooi, Evaporation and dispersion of respiratory droplets from coughing, *Indoor Air.* 27 (2017) 179–190.
- [21] X. Li, Y. Shang, Y. Yan, L. Yang, J. Tu, Modelling of evaporation of cough droplets in inhomogeneous humidity fields using the multi-component Eulerian-Lagrangian approach, *Build. Environ.* 128 (2018) 68–76.
- [22] Y. Yan, X. Li, J. Tu, Thermal effect of human body on cough droplets evaporation and dispersion in an enclosed space, *Build. Environ.* 148 (2019) 96–106.
- [23] X. Yang, C. Ou, H. Yang, L. Liu, T. Song, M. Kang, H. Lin, J. Hang, Transmission of pathogen-laden expiratory droplets in a coach bus, *J. Hazard. Mater.* 397 (2020) 122609.
- [24] L. Zhang, Y. Li, Dispersion of coughed droplets in a fully-occupied high-speed rail cabin, *Build. Environ.* 47 (2012) 58–66.
- [25] K.W. Mui, L.T. Wong, C.L. Wu, A.C.K. Lai, Numerical modeling of exhaled droplet nuclei dispersion and mixing in indoor environments, *J. Hazard. Mater.* 167 (2009) 736–744.
- [26] B. Zhao, J. Wu, Effect of particle spatial distribution on particle deposition in ventilation rooms, *J. Hazard. Mater.* 170 (2009) 449–456.
- [27] Z. Lin, J. Wang, T. Yao, T.T. Chow, Investigation into anti-airborne infection performance of stratum ventilation, *Build. Environ.* 54 (2012) 29–38.
- [28] Q. He, J. Niu, N. Gao, T. Zhu, J. Wu, CFD study of exhaled droplet transmission between occupants under different ventilation strategies in a typical office room, *Build. Environ.* 46 (2011) 397–408.
- [29] T.-H. Shih, W.W. Liou, A. Shabbir, Z. Yang, J. Zhu, A new  $k-\epsilon$  eddy viscosity model for high Reynolds number turbulent flows, *Computers Fluids.* 24 (1995) 227–238.
- [30] B.P. Leonard, A stable and accurate convective modelling procedure based on quadratic upstream interpolation, *Comput. Methods Appl. Mech. Eng.* 19 (1979) 59–98.
- [31] C. Gromke, B. Blocken, W. Janssen, B. Merema, T. van Hooff, H. Timmermans, CFD analysis of transpirational cooling by vegetation: Case study for specific meteorological conditions during a heat wave in Arnhem, Netherlands, *Build. Environ.* 83 (2015) 11–26.

- [32] T. van Hooff, B. Blocken, Coupled urban wind flow and indoor natural ventilation modelling on a high-resolution grid: A case study for the Amsterdam ArenA stadium, *Environ. Model. Softw.* 25 (2010) 51–65.
- [33] H. Montazeri, B. Blocken, J.L.M. Hensen, Evaporative cooling by water spray systems: CFD simulation, experimental validation and sensitivity analysis, *Build. Environ.* 83 (2015) 129–141.
- [34] H. Montazeri, Y. Toparlar, B. Blocken, J.L.M. Hensen, Simulating the cooling effects of water spray systems in urban landscapes: A computational fluid dynamics study in Rotterdam, The Netherlands, *Landsc. Urban Plan.* 159 (2017) 85–100.
- [35] L. Schiller, A. Naumann, Über die grundlegenden berechnungen bei der schwerkraftaufbereitung, *Zeitschrift Des Vereines Dtsch. Ingenieure.* (1933).
- [36] Y.S. Cheng, M.D. Allen, D.P. Gallegos, H.C. Yeh, K. Peterson, Drag force and slip correction of aggregate aerosols, *Aerosol Sci. Technol.* 8 (1988) 199–214.
- [37] A.D. Gosman, E. Ioannides, Aspects of computer simulation of liquid-fueled combustors, *J. Energy.* (1983).
- [38] P. V. Nielsen, Computational fluid dynamics and room air movement, *Indoor Air.* 14 (2004) 134–143.
- [39] N. Dudalski, A. Mohamed, S. Mubareka, R. Bi, C. Zhang, E. Savory, Experimental investigation of far-field human cough airflows from healthy and influenza-infected subjects, *Indoor Air.* 30 (2020) 966–977.
- [40] H. Qian, Y. Li, Removal of exhaled particles by ventilation and deposition in a multibed airborne infection isolation room, *Indoor Air.* 20 (2010) 284–297.
- [41] W. Oh, R. Ooka, H. Kikumoto, M. Han, Numerical modeling of cough airflow: Establishment of spatial-temporal experimental dataset and CFD simulation method, *Build. Environ.* 207 (2022) 108531.
- [42] H. Holmgren, B. Bake, A. Olin, E. Ljungström, Relation between humidity and size of exhaled particles, *J. Aerosol Med. Pulm. Drug Deliv.* 24 (2011) 253–260.